Geophysical Research Letters

RESEARCH LETTER
10.1029/2019GL082172

The 2005–2016 Trends of Formaldehyde Columns Over China Observed by Satellites: Increasing Anthropogenic Emissions of Volatile Organic Compounds and Decreasing Agricultural Fire Emissions

Lu Shen[1], Daniel J. Jacob[1], Lei Zhu[1,2], Qiang Zhang[3], Bo Zheng[4], Melissa P. Sulprizio[1], Ke Li[1], Isabelle De Smedt[5], Gonzalo González Abad[2], Hansen Cao[6], Tzung-May Fu[7], and Hong Liao[8]

[1]John A. Paulson School of Engineering and Applied Sciences, Harvard University, Cambridge, MA, USA, [2]Atomic and Molecular Physics Division, Harvard-Smithsonian Center for Astrophysics, Cambridge, MA, USA, [3]Ministry of Education Key Laboratory for Earth System Modeling, Department of Earth System Science, Tsinghua University, Beijing, China, [4]Laboratoire des Sciences du Climat et de l'Environnement, CEA-CNRS-UVSQ, UMR8212, Gif-sur-Yvette, France, [5]Belgian Institute for Space Aeronomy (BIRA-IASB), Brussels, Belgium, [6]Department of Mechanical Engineering, University of Colorado, Boulder, CO, USA, [7]Department of Atmospheric and Oceanic Sciences, School of Physics, Peking University, Beijing, China, [8]School of Environmental Science and Engineering, Nanjing University of Information Science and Technology, Nanjing, China

Abstract We use 2005–2016 observations of formaldehyde (HCHO) columns over China from the OMI, GOME-2, and SCIAMACHY satellite instruments to evaluate long-term trends in emission inventories of volatile organic compounds (VOCs) that affect air quality. The observations show large increases over 2005–2016 in the North China Plain ($+1.1 \pm 0.5\%$ a^{-1} relative to 2005) and the Yangtze River Delta region ($+1.5 \pm 0.4\%$ a^{-1} relative to 2005), consistent with the trend of anthropogenic VOC emissions in the Multi-resolution Emission Inventory for China (MEIC). Unlike other pollutants, VOC emissions have not been decreasing in recent years. An exception is the Huai River Basin in rural eastern China where the satellite data show rapidly decreasing VOC emissions since the early 2010s that appear to reflect bans on agricultural fires.

Plain Language Summary Satellite observations of formaldehyde can detect emissions of volatile organic compounds (VOCs), which are of concern for air quality. Here we use 2005–2016 satellite observations of formaldehyde over China to infer trends in VOC emissions. We find increases of 13% in the North China Plain and 18% in the Yangtze River Delta. Unlike other pollutants, emissions of VOCs in China have not decreased in recent years. An exception is in rural areas where post-2010 restrictions on crop burning to improve air quality have resulted in sharp decreases of VOC emissions.

Key Points:
- 2005 to 2016 satellite observations of formaldehyde show increases in Chinese anthropogenic emissions of volatile organic compounds
- The increases are largest in the North China Plain and Yangtze River Delta and are consistent with the MEIC emission inventory
- Decreases are observed in rural eastern China since the early 2010s that appear due to new restrictions on crop burning

Supporting Information:
- Supporting Information S1

Correspondence to:
L. Shen,
lshen@fas.harvard.edu

Citation:
Shen, L., Jacob, D. J., Zhu, L., Zhang, Q., Zheng, B., Sulprizio, M. P., et al. (2019). The 2005–2016 trends of formaldehyde columns over China observed by satellites: Increasing anthropogenic emissions of volatile organic compounds and decreasing agricultural fire emissions. *Geophysical Research Letters*, *46*. https://doi.org/10.1029/2019GL082172

Received 23 JAN 2019
Accepted 26 MAR 2019
Accepted article online 1 APR 2019

1. Introduction

Volatile organic compounds (VOCs) affect air quality by producing ozone and organic particulate matter. They are emitted by anthropogenic, pyrogenic, and biogenic sources, and they are oxidized in the atmosphere by the hydroxyl radical (OH) with a range of lifetimes. Highly reactive VOCs with lifetimes of less than a day are particularly relevant for air quality (Wert et al., 2003). Oxidation of these highly reactive VOCs produces formaldehyde (HCHO) near the emission sources. HCHO columns can be observed by satellites and from there the rate of VOC emissions can be inferred (Barkley et al., 2013; Marais et al., 2012; Palmer et al., 2003; Stavrakou et al., 2009; Zhu et al., 2014; Zhu, Jacob, et al., 2017). Major efforts have been underway in China over the past decade to reduce pollution and this has led to large decreases in emissions, but inventory estimates suggest that VOC emissions have not decreased (Zheng et al., 2018). Here we examine 2005–2016 trends of HCHO in China as observed from space by the OMI, SCIAMACHY, and GOME-2 instruments, and we infer from there the long-term changes of VOC emissions over that period.

Quantifying anthropogenic VOC emissions in process-based inventories is difficult because the processes involved include leaks, volatilization, and incomplete combustion, with highly uncertain emission factors (Zheng et al., 2018). Crop residue burning may also be a large seasonal source of VOCs in parts of China

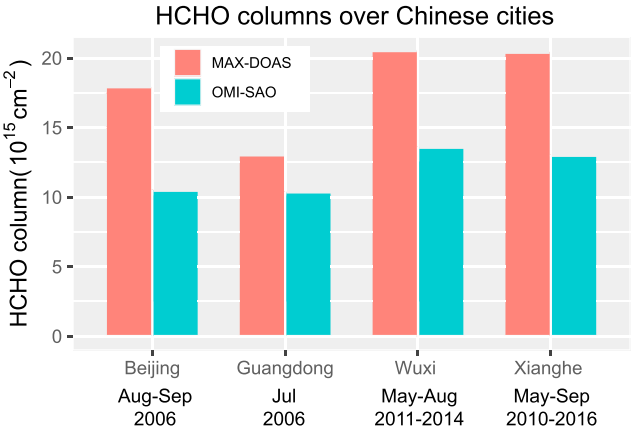

Figure 1. Evaluation of the OMI-SAO HCHO column data with mean ground-based MAX-DOAS column measurements over four cities in China. The ground-based measurements are from Li et al. (2013), Lee et al. (2015), Vlemmix et al. (2015), and Wang et al. (2017), as compiled in Table S3 of Cao et al. (2018). The OMI-SAO data are means for the observation period. HCHO = formaldehyde.

(Cao et al., 2018; Huang et al., 2012) but is poorly quantified (Huang et al., 2012; van der Werf et al., 2010; Zhang et al., 2016). Biogenic emissions by vegetation, in particular of isoprene, are an additional source of VOCs (Fu & Liao, 2012; Guenther et al., 2006). A number of studies have used HCHO observations from space to infer VOC emissions and test inventories (Palmer et al., 2003; Stavrakou et al., 2009; Zhu et al., 2014), including specifically for China (Cao et al., 2018; Chan Miller et al., 2016; Fu et al., 2007). De Smedt et al. (2010) found a 3% a^{-1} HCHO increase over China between 1997 and 2009 that they attributed to changes in VOC emissions. Our work extends the trend analysis to more recent years including the spatial distribution across eastern China with focus on separating anthropogenic, pyrogenic, and biogenic contributions.

2. Data and Methods

The core of our analysis is based on the OMI HCHO Level 2 product (Collection 3) from the Smithsonian Astrophysical Observatory (OMI-SAO), as described by González Abad et al. (2015). OMI is a UV/Vis nadir solar backscatter spectrometer launched in 2004 and provides daily global observations at a 13×24 km^2 nadir pixel resolution with a local equator crossing time of 13:38 (Levelt et al., 2006). HCHO slant columns are fitted using backscattered solar radiation within the 328.5–356.5 nm band and converted to vertical columns using air mass factors based on vertical profiles from the GEOS-Chem model (González Abad et al., 2015). Similar to Zhu et al. (2014), we only use observations that (1) pass all quality checks, (2) have a cloud fraction less than 0.3 and solar zenith angle less than 60°, and (3) are from rows 1–20 and 55–60 of the OMI detector that are not affected by the row anomalies (Kroon et al., 2011). The daily HCHO columns are then averaged on a $0.5° \times 0.5°$ grid to yield a 12-year monthly product for 2005–2016. We focus on May–September when prompt oxidation of VOCs provides the strongest HCHO signal (Zhu, Mickley, et al., 2017; Zhu, Jacob, et al., 2017). Lower oxidant concentrations in winter leads to smearing and dilution of the signal below the detection limit of 1×10^{16} molecules cm^{-2} (González Abad et al., 2015; Zhu et al., 2014). There is a well-known global background drift in the OMI data that we correct following Marais et al. (2012), Zhu, Mickley, et al. (2017), and Zhu, Jacob, et al. (2017) by subtracting a smoothed trend of HCHO column over the remote North Pacific (180–150°W, 10–55°N). The average linear trend of this drift is 4.3×10^{13} molecules cm^{-2} a^{-1} during 2005–2016, compared to 9×10^{12} molecules cm^{-2} a^{-1} in the GEOS-Chem model (mainly from the growth of methane). The regional HCHO trends over China presented in the next section after removal of this drift are of order $1–3 \times 10^{14}$ molecules cm^2 a^{-1}.

Validation with aircraft and ground-based measurements shows that the OMI-SAO HCHO columns have a uniform 40% low bias and that other satellite HCHO products have similar biases (Barkley et al., 2013; De Smedt et al., 2015; Zhu et al., 2016), possibly due to common errors in spectral fitting. Validation by Zhu et al. (2016) over the Southeast United States suggests that this bias is uniform and can be remedied with a correction factor. Figure 1 compares the OMI-SAO data with ground-based MAX-DOAS column measurements in four Chinese cities (Lee et al., 2015; Li et al., 2013; Wang et al., 2017). Assuming that the MAX-DOAS measurements are representative of the ~20 km OMI pixel scale, we find a mean 33% low bias in OMI, consistent with past work. On that basis we apply a uniform correction factor of 1.5 (i.e., 1/(1–0.33)) to the OMI-SAO data.

We compare the OMI-SAO HCHO trends with data from other satellite instruments and retrievals available from the Belgian Institute for Space Aeronomy (BIRA) at http://h2co.aeronomie.be/. These include SCIAMACHY for 2002–2011 (De Smedt et al., 2008; Wittrock et al., 2006), GOME-2 on MetOp-A for 2007–2013 and MetOp-B for 2013-present (De Smedt et al., 2012; Hewson et al., 2015), and the OMI retrieval developed by BIRA for 2005–2016 (OMI-BIRA, De Smedt et al., 2015). The overpass local solar time is roughly 13:30 for OMI and 9:30 for GOME-2 and SCIAMACHY. We multiply the GOME-2 HCHO columns in MetOp-A by 1.19 to match the mean 2013 HCHO columns observed by MetOp-B over eastern China (110–125°E, 21–42°N), and then we combine these two into a single GOME-2 data set. We multiply the

SCIAMACHY, GOME-2, and OMI-BIRA products by constant scaling factors (1.40, 1.31, 1.32) to match the bias-corrected OMI-SAO data over the same eastern China domain during 2007–2011 (an overlapping period for all products). Diurnal variation of HCHO columns between 9:30 and 13:30 is thought to be only a few percent (Millet et al., 2008).

We use the Multi-resolution Emission Inventory for China (MEIC, Zheng et al., 2018) as bottom-up estimate of anthropogenic VOC emissions. MEIC incorporates detailed provincial activity rates and emission factors for a variety of sources and for individual years. For open fire emissions, we use the Fire INventory from NCAR (FINN version 1.5, Wiedinmyer et al., 2011), which is based on fire counts from the MODIS satellite instrument. Fire emissions peak in June after the wheat harvest (Stavrakou et al., 2016; Zhang et al., 2016). For biogenic emissions we use the MEGAN v2.1 inventory of Guenther et al. (2012) as implemented in GEOS-Chem by Hu et al. (2017). All data are available for 2005–2016.

We perform a 12-year simulation (2005–2016) with the 2° × 2.5° GEOS-Chem global model of atmospheric chemistry (v11-02, http://geos-chem.org) to relate trends of anthropogenic VOC emissions to trends of HCHO columns. The model is driven by MERRA2 assimilated meteorological data (Gelaro et al., 2017). Anthropogenic and open fire emissions are from MEIC and FINN. Biogenic VOC emissions for all years are computed with MEGAN v2.1. We neglect any changes in land cover that would drive a trend in biogenic HCHO.

The biogenic source has a large temperature dependence that is apparent in the interannual variability (IAV) of HCHO column observations (Palmer et al., 2006; Zhu et al., 2014) and can obfuscate long-term trend analysis (Zhu, Mickley, et al., 2017). Here we remove this dependence in the OMI data following Zhu, Mickley, et al. (2017) by regressing the May–September monthly mean HCHO columns onto midday surface air temperatures for 2005–2016 in each grid cell, and subtracting the fitted temperature dependency from the original data (Figure S1).

3. Results and Discussion

Figure 2 shows the mean May–September OMI HCHO columns over China for 2005–2016. Values exceed 15×10^{15} molecules cm^{-2} in megacity clusters, such as in the North China Plain (NCP), Pearl River Delta, Yangtze River Delta (YRD), and the Sichuan Basin. Also shown in Figure 2 are the HCHO production rates from anthropogenic, biogenic, and open fire VOCs, as estimated by applying 1-day HCHO production yields under high-NO_x conditions (Chan Miller et al., 2016) to emissions of individual VOCs from the bottom-up MEIC, MEGAN, and FINN inventories, respectively. The 1-day HCHO yields of individual VOCs and their contributions to the mean HCHO columns over China in May–September are listed in Table S1. The principal anthropogenic VOC contributors to HCHO are alkanes (49%), alkenes (34%), and aromatics (10%). The principal open fire VOC contributors are alkanes (40%), carbonyls (34%), and alkenes (21%). The principal biogenic VOC contributors are isoprene (73%), monoterpenes (12%), and propene (9%).

We see from Figure 2 that the observed OMI HCHO distribution follows that expected from the MEIC anthropogenic inventory, with high values found in megacity clusters. It does not follow the biogenic source from MEGAN, which contributes more HCHO over eastern China during May–September (8.6 vs 5.5 Tg), but it is more broadly distributed. This contrasts with the United States where OMI HCHO distribution closely matches the MEGAN biogenic source pattern because the anthropogenic source is considerably lower (Millet et al., 2008). The open fire source from FINN follows the distribution of cropland (Xie et al., 2016) but is much smaller (0.58 Tg) than the anthropogenic and biogenic sources.

Figure 3a shows the May–September 2005–2016 trends of OMI HCHO columns after correcting for the temperature dependence. We find that HCHO columns increase at a mean rate of $0.22 \pm 0.06 \times 10^{15}$ molecules cm^{-2} a^{-1} ($+1.8 \pm 0.5\%$ a^{-1} relative to 2005) in the NCP and $0.20 \pm 0.07 \times 10^{15}$ molecules cm^{-2} a^{-1} ($+1.6 \pm 0.6\%$ a^{-1}) in the YRD. In between these two regions, we find decreasing trends in the Huai River Basin (HRB) where emissions from agricultural fires are concentrated (Figure 2). The multisatellite mean show similar spatial patterns of these trends during 2005–2016, with similar trends in YRD ($+1.5 \pm 0.4\%$ a^{-1}), lower trends in NCP ($+1.1 \pm 0.5\%$ a^{-1}) and decreasing trends in HRB (Figure S2). Also shown in Figure 3 are the 2005–2016 trends simulated by GEOS-Chem on the 2° × 2.5° grid. GEOS-Chem

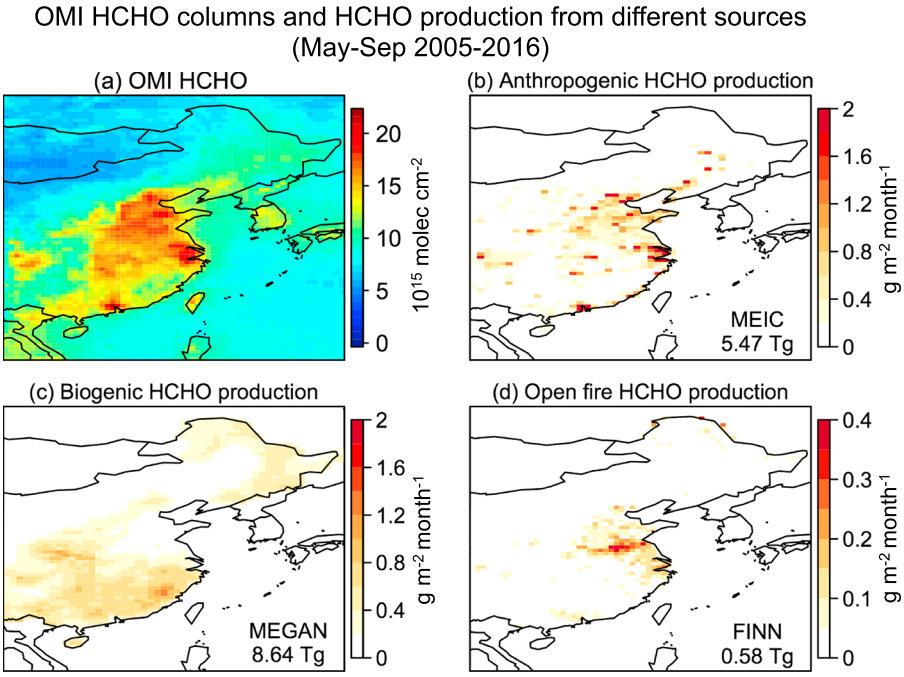

Figure 2. Mean HCHO over China in May–September 2005–2016 and its sources as estimated from bottom-up emission inventories of nonmethane VOCs. (a) HCHO columns from the OMI-SAO satellite retrieval with bias correction applied (section 2). (b) Mean anthropogenic production rate derived from MEIC VOC emissions with 1-day HCHO yields. (c) Same as (b) but for biogenic emissions from MEGAN v2.1 driven by 2005 MERRA2 meteorology. (d) Same as (b) but for open fires from FINN. Note the lower scale for open fire emissions. The HCHO 1-day yields from oxidation of different VOC species are from Chan Miller et al. (2016), as given in Table S1. The May–September total HCHO production amounts during 2005–2016 from each source type in eastern China (east of 103°E, covering the map domain) are shown inset. HCHO = formaldehyde; VOC = volatile organic compound; MEIC = Multi-resolution Emission Inventory for China; FINN = Fire INventory from NCAR.

can capture the general increases observed by OMI over the NCP and YRD when smoothed over the 2° × 2.5° model grid but fails at reproducing the decrease over HRB.

The HCHO trends in GEOS-Chem are driven by MEIC anthropogenic emissions and FINN open fire emissions. Figure 4 shows the 2005–2016 linear trends of these emissions. MEIC shows the largest anthropogenic

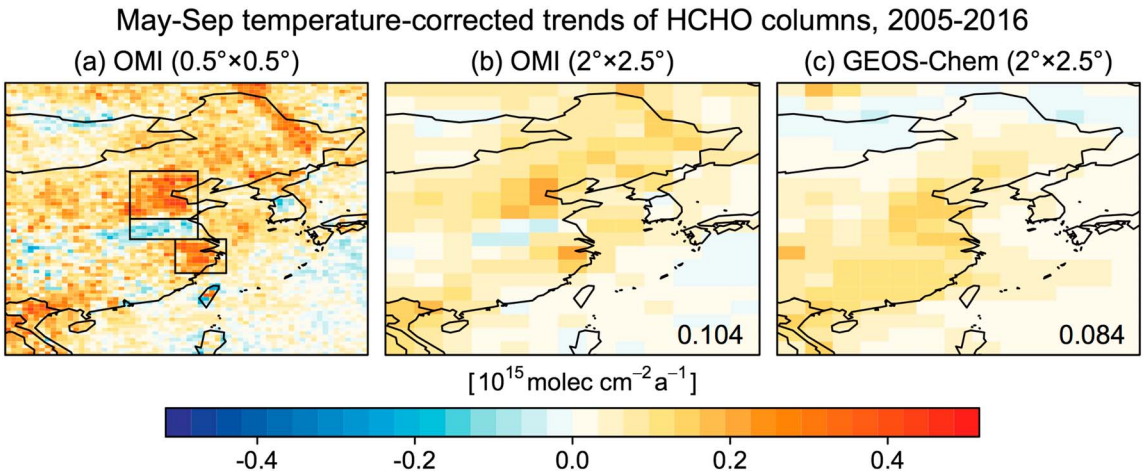

Figure 3. The 2005–2016 trends of formaldehyde (HCHO) columns over China. Values are fitted linear trends for May–September 5-month averages of each year. OMI trends are corrected for temperature as described in the text. (a) Observed OMI trends on the 0.5° × 0.5° grid. From top to bottom, the three rectangles delineate the North China Plain, Huai River Basin, and Yangtze River Delta. (b) Same as (a) but on a 2° × 2.5° grid. (c) 2005–2016 trends simulated by GEOS-Chem at 2° × 2.5° resolution with fixed biogenic sources at the 2005 level. The averaged trends in eastern China are shown inset.

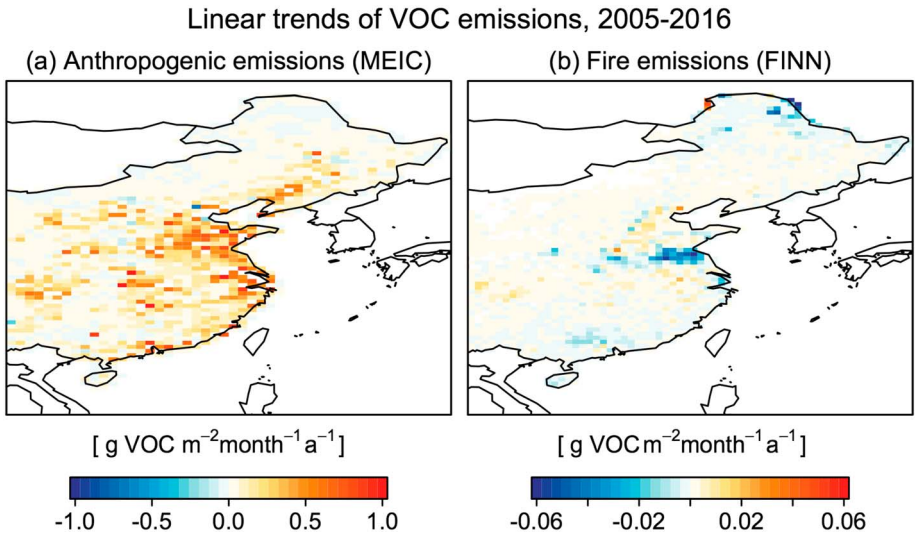

Figure 4. The 2005–2016 trends of May–September VOC emissions from anthropogenic (MEIC) and open fire (FINN) inventories, plotted on the same 0.5° × 0.5° grid as OMI formaldehyde in Figure 3a. Note the smaller scale for open fire emissions. VOC = volatile organic compound; MEIC = Multi-resolution Emission Inventory for China; FINN = Fire INventory from NCAR.

increases in the NCP and YRD, corresponding to the regions of maximum OMI HCHO increases in Figure 3a. The MEIC-driven model increases relative to 2005 are +1.0 ± 0.3% a^{-1} in the NCP and +1.0 ± 0.2% a^{-1} in YRD, consistent with the satellite trends and implying consistency of the satellite and MEIC emission trends. FINN shows a decrease in open fire emissions in the HRB, matching closely the pattern of OMI HCHO decrease in that region, and reflecting recent bans on agricultural fires because of concerns over air quality (Zhang et al., 2016; Zhuang et al., 2018). The magnitude of the decreasing trend in FINN open fire emissions is however much smaller than the increase in MEIC anthropogenic emissions (note the different scales in Figure 4), explaining why GEOS-Chem does not capture the localized HCHO decrease in the HRB observed by OMI.

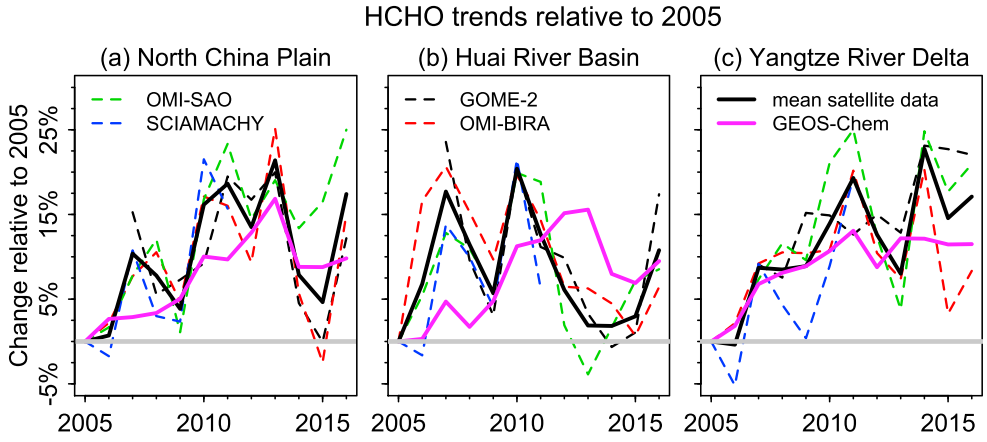

Figure 5. The 2005–2016 time series of mean May–September HCHO columns from different satellite products over the North China Plain, Huai River Basin, and Yangtze River Delta. HCHO columns are shown as the changes relative to 2005 (gray horizontal line) after correcting the temperature dependence of biogenic sources and the Pacific background, as described in the text. The individual satellite products have been adjusted by 30–40% to match the mean bias-corrected OMI-SAO data for 2007–2011 (see text). GOME-2 only operates after 2007, so we calculate its changes relative to OMI-SAO columns in 2005. The three regions are defined in Figure 3a. Individual satellite products are shown as dashed lines and the mean of all products is the black bold line. Also shown is the trend in the GEOS-Chem simulation driven by the Multi-resolution Emission Inventory for China anthropogenic and Fire INventory from NCAR open fire inventories. HCHO = formaldehyde.

The HCHO yield from oxidation of VOCs increases with increasing nitrogen oxides ($NO_x \equiv NO + NO_2$). NO_x emissions in China increased by 40% over 2005–2011 and then decreased by 25% over 2011–2016 according to MEIC and as implemented in GEOS-Chem (Figure S3a). We examined the effect on the HCHO trend by conducting a 12-year sensitivity simulation with NO_x emissions fixed at the 2005 level. The simulated trend of HCHO columns in eastern China relative to 2005 is 1.0% a^{-1}, very similar to the trend of 1.1% a^{-1} with varying NO_x emissions (Figure S3b). This is because the prompt HCHO yield is relatively insensitive to NO_x emission changes in the high-NO_x regime (Chan Miller et al., 2017).

The inability of GEOS-Chem to reproduce the observed OMI HCHO decrease over the HRB suggests that FINN open fire emissions may be too low, consistent with Cao et al. (2018). Burning in that region is from small agricultural plots and this may be poorly detected by MODIS either as fire counts or burned area (Huang et al., 2012; van der Werf et al., 2010; Zhang et al., 2016). The frequently used Global Fire Emissions Database version 4 with small fires (GFED4s, van der Werf et al., 2017), also relying on MODIS, is three times lower than FINN over the HRB. An inverse analysis of OMI HCHO data by Stavrakou et al. (2016) for eastern China finds open fire emissions three to four times higher than FINN.

We have so far analyzed linear trends over the 2005–2016 period, but the MEIC and FINN inventory trends show significant nonlinearity (Figure S4). Anthropogenic emissions grew at a weaker rate after 2010 and leveled off in the NCP. Open fire emissions began to decrease only after 2012 and dropped to nearly zero by 2016.

Figure 5 addresses this nonlinearity in the trend by showing the annual changes relative to 2005 of HCHO columns in our three target regions and including other satellite products in addition to OMI-SAO. We find good consistency between satellite products in the long-term trends and IAV, reflecting the robustness of temporal trends in the satellite data when averaged spatially on a regional scale (Zhu et al., 2016). The model represents well the long-term trends in NCP and YRD, including the leveling off after 2010 apparent from the MEIC and FINN inventories (Figure S4). The satellite data show fairly consistent 5–10% IAV in NCP and YRD superimposed on the long-term trend but the model does not reproduce that. This suggests more year-to-year variation in VOC emissions than indicated by MEIC. The relatively low values observed in 2009 could reflect the economic recession. There could also be IAV from agricultural fires not accounted in FINN. The observed IAV in the HRB is much larger than in NCP or YRD, as might be expected from fire emissions, and the decrease starts after 2010 which is consistent with the ban on agricultural fires. We find that this decreasing trend in the HRB data after 2010 is most pronounced in June which is the peak fire month (Figure S5). The inability of the model to reproduce the amplitude of this decrease is consistent with the FINN fire emissions being too low.

In summary, we have used temperature-corrected 2005–2016 (May–September) trends of formaldehyde (HCHO) columns observed by satellites (OMI, GOME-2, SCIAMACHY) over China to evaluate VOC emission trends reported in anthropogenic and open fire emission inventories. The different satellite products indicate generally consistent trends and variability. They show increasing trends of HCHO columns across much of eastern China over 2005–2016, especially in the NCP (+1.1 ± 0.5% a^{-1} relative to 2005) and YRD (+1.5 ± 0.4% a^{-1}). These trends are consistent with the MEIC anthropogenic VOC emission inventory. The MEIC inventory finds a leveling of VOC emission trends after 2010 and this is indeed seen in the satellite data. Unlike other pollutants like SO_2 or NO_x, VOC emissions in China have not been decreasing in recent years. An exception is the HRB, where the satellite instruments show a decrease over the 2005–2016 period though with large IAV. This is a region where considerable crop residue burning used to take place until the early 2010s but has since been banned because of air quality concerns. The decreasing trend seen in the HCHO satellite data for that region implies much higher open fire emissions in the pre-2012 period than estimated in the FINN and GFED4 inventories.

Acknowledgments
This work was funded by the Harvard Global Institute (HGI), the NASA Earth Science Division, and the Joint Laboratory for Air Quality and Climate (JLAQC) between Harvard and the Nanjing University for Information Science and Technology (NUIST). All data used in this study are publically accessible. All data used in this study can be accessed via doi (https://doi.org/10.7910/DVN/ALHRX1).

References

Barkley, M. P., Smedt, I. D., van Roozendael, M., Kurosu, T. P., Chance, K., Arneth, A., et al. (2013). Top-down isoprene emissions over tropical South America inferred from SCIAMACHY and OMI formaldehyde columns. *Journal of Geophysical Research: Atmospheres*, *118*, 6849–6868. https://doi.org/10.1002/jgrd.50552

Cao, H., Fu, T. M., Zhang, L., Henze, D. K., Miller, C. C., Lerot, C., et al. (2018). Adjoint inversion of Chinese non-methane volatile organic compound emissions using space-based observations of formaldehyde and glyoxal. *Atmospheric Chemistry and Physics*, *18*, 15,017–15,046. https://doi.org/10.5194/acp-18-15017-2018

Chan Miller, C., Jacob, D. J., Marais, E. A., Yu, K., Travis, K. R., Kim, P. S., et al. (2016). Glyoxal yield from isoprene oxidation and relation to formaldehyde: Chemical mechanism, constraints from SENEX aircraft observations, and interpretation of OMI satellite data. *Atmospheric Chemistry and Physics Discussions*, 1–25. https://doi.org/10.5194/acp-2016-1042

Chan Miller, C., Jacob, D. J., Marais, E. A., Yu, K., Travis, K. R., Kim, P. S., et al. (2017). Glyoxal yield from isoprene oxidation and relation to formaldehyde: Chemical mechanism, constraints from SENEX aircraft observations, and interpretation of OMI satellite data. *Atmospheric Chemistry and Physics*, *17*, 8725–8738. https://doi.org/10.5194/acp-17-8725-2017

De Smedt, I., Müller, J.-F., Stavrakou, T., van der A, R., Eskes, H., & van Roozendael, M. (2008). Twelve years of global observations of formaldehyde in the troposphere using GOME and SCIAMACHY sensors. *Atmospheric Chemistry and Physics*, *8*, 4947–4963. https://doi.org/10.5194/acp-8-4947-2008

De Smedt, I., Stavrakou, T., Hendrick, F., Danckaert, T., Vlemmix, T., Pinardi, G., et al. (2015). Diurnal, seasonal and long-term variations of global formaldehyde columns inferred from combined OMI and GOME-2 observations. *Atmospheric Chemistry and Physics*, *15*(21), 12,519–12,545. https://doi.org/10.5194/acp-15-12519-2015

De Smedt, I., Stavrakou, T., Müller, J.-F., van der Abo, R. J., & van Roozendael, M. (2010). Trend detection in satellite observations of formaldehyde tropospheric columns. *Geophysical Research Letters*, *37*, L18808. https://doi.org/10.1029/2010GL044245

De Smedt, I., Van Roozendael, M., Stavrakou, T., Müller, J. F., Lerot, C., Theys, N., et al. (2012). Improved retrieval of global tropospheric formaldehyde columns from GOME-2/MetOp-A addressing noise reduction and instrumental degradation issues. *Atmospheric Measurement Techniques*, *5*(11), 2933–2949. https://doi.org/10.5194/amt-5-2933-2012

Fu, T.-M., Jacob, D. J., Palmer, P. I., Chance, K., Wang, Y. X., Barletta, B., et al. (2007). Space-based formaldehyde measurements as constraints on volatile organic compound emissions in east and South Asia and implications for ozone. *Journal of Geophysical Research*, *112*, D06312. https://doi.org/10.1029/2006JD007853

Fu, Y., & Liao, H. (2012). Simulation of the interannual variations of biogenic emissions of volatile organic compounds in China: Impacts on tropospheric ozone and secondary organic aerosol. *Atmospheric Environment*, *59*, 170–185. https://doi.org/10.1016/j.atmosenv.2012.05.053

Gelaro, R., McCarty, W., Suárez, M. J., Todling, R., Molod, A., Takacs, L., et al. (2017). The modern-era retrospective analysis for research and applications, version 2 (MERRA-2). *Journal of Climate*, *30*(14), 5419–5454. https://doi.org/10.1175/JCLI-D-16-0758.1

González Abad, G., Liu, X., Chance, K., Wang, H., Kurosu, T. P., & Suleiman, R. (2015). Updated Smithsonian Astrophysical Observatory Ozone Monitoring Instrument (SAO OMI) formaldehyde retrieval. *Atmospheric Measurement Techniques*, *8*, 19–32. https://doi.org/10.5194/amt-8-19-2015

Guenther, A. B., Jiang, X., Heald, C. L., Sakulyanontvittaya, T., Duhl, T., Emmons, L. K., & Wang, X. (2012). The model of emissions of gases and aerosols from nature version 2.1 (MEGAN2.1): An extended and updated framework for modeling biogenic emissions. *Geoscientific Model Development*, *5*, 1471–1492. https://doi.org/10.5194/gmd-5-1471-2012

Guenther, A., Karl, T., Harley, P., Wiedinmyer, C., Palmer, P. I., & Geron, C. (2006). Estimates of global terrestrial isoprene emissions using MEGAN (model of emissions of gases and aerosols from nature). *Atmospheric Chemistry and Physics*, *6*, 3181–3210. https://doi.org/10.5194/acp-6-3181-2006

Hewson, W., Barkley, M. P., Gonzalez Abad, G., Bösch, H., Kurosu, T., & Spurr, R. (2015). Development and characterisation of a state- of-the-art GOME-2 formaldehyde air-mass factor algorithm. *Atmospheric Measurement Techniques*, *8*, 4055–4074. https://doi.org/10.5194/amt-8-4055-2015

Hu, L., Jacob, D. J., Liu, X., Zhang, Y., Zhang, L., Kim, P. S., et al. (2017). Global budget of tropospheric ozone: Evaluating recent model advances with satellite (OMI), aircraft (IAGOS), and ozonesonde observations. *Atmospheric Environment*, *167*, 323–334. https://doi.org/10.1016/j.atmosenv.2017.08.036

Huang, X., Li, M., Li, J., & Song, Y. (2012). A high resolution emission inventory of crop burning in field in China based on MODIS thermal anomalies/fire products. *Atmospheric Environment*, *50*, 9–15. https://doi.org/10.1016/j.atmosenv.2012.01.017

Kroon, M., de Haan, J. F., Veefkind, J. P., Froidevaux, L., Wang, R., Kivi, R., & Hakkarainen, J. J. (2011). Validation of operational ozone profiles from the ozone monitoring instrument. *Journal of Geophysical Research*, *116*, D18305. https://doi.org/10.1029/2010JD015100

Lee, H., Ryu, J., Irie, H., Jang, S.-H., Park, J., Choi, W., & Hong, H. (2015). Investigations of the diurnal variation of vertical HCHO profiles based on MAX-DOAS measurements in Beijing: Comparisons with OMI vertical column data. *Atmosphere*, *6*, 1816–1832. https://doi.org/10.3390/atmos6111816

Levelt, P. F., van den Oord, G. H. J., Dobber, M. R., Malkki, A., Visser, H., de Vries, J., et al. (2006). The ozone monitoring instrument. *IEEE Transactions on Geoscience and Remote Sensing*, *44*(5), 1093–1101. https://doi.org/10.1109/TGRS.2006.872333

Li, X., Brauers, T., Hofzumahaus, A., Lu, K., Li, Y. P., Shao, M., et al. (2013). MAX-DOAS measurements of NO2, HCHO and CHOCHO at a rural site in southern China. *Atmospheric Chemistry and Physics*, *13*, 2133–2151. https://doi.org/10.5194/acp-13-2133-2013

Marais, E. A., Jacob, D. J., Kurosu, T. P., Chance, K., Murphy, J. G., Reeves, C., et al. (2012). Isoprene emissions in Africa inferred from OMI observations of formaldehyde columns. *Atmospheric Chemistry and Physics*, *12*, 6219–6235. https://doi.org/10.5194/acp-12-6219-2012

Millet, D. B., Jacob, D. J., Boersma, K. F., Fu, T. M., Kurosu, T. P., Chance, K., et al. (2008). Spatial distribution of isoprene emissions from North America derived from formaldehyde column measurements by the OMI satellite sensor. *Journal of Geophysical Research*, *113*, D02307. https://doi.org/10.1029/2007JD008950

Palmer, P. I., Abbot, D. S., Fu, T. M., Jacob, D. J., Chance, K., Kurosu, T. P., et al. (2006). Quantifying the seasonal and interannual variability of North American isoprene emissions using satellite observations of the formaldehyde column. *Journal of Geophysical Research*, *111*, D12315. https://doi.org/10.1029/2005JD006689

Palmer, P. I., Jacob, D. J., Fiore, A. M., Martin, R. V., Chance, K., & Kurosu, T. P. (2003). Mapping isoprene emissions over North America using formaldehyde column observations from space. *Journal of Geophysical Research*, *108*(D6), 4180. https://doi.org/10.1029/2002JD002153

Stavrakou, T., Müller, J. F., Bauwens, M., De Smedt, I., Lerot, C., van Roozendael, M., et al. (2016). Substantial underestimation of post-harvest burning emissions in the North China plain revealed by multi-species space observations. *Scientific Reports*, *6*, 32307. https://doi.org/10.1038/srep32307

Stavrakou, T., Müller, J.-F., De Smedt, I., van Roozendael, M., van der Werf, G. R., Giglio, L., & Guenther, A. (2009). Global emissions of non-methane hydrocarbons deduced from SCIAMACHY formaldehyde columns through 2003–2006. *Atmospheric Chemistry and Physics*, *9*, 3663–3679. https://doi.org/10.5194/acp-9-3663-2009

van der Werf, G. R., Randerson, J. T., Giglio, L., Collatz, G. J., Mu, M., Kasibhatla, P. S., et al. (2010). Global fire emissions and the contribution of deforestation, savanna, forest, agricultural, and peat fires (1997–2009). *Atmospheric Chemistry and Physics*, *10*, 11,707–11,735. https://doi.org/10.5194/acp-10-11707-2010

van der Werf, G. R., Randerson, J. T., Giglio, L., van Leeuwen, T. T., Chen, Y., Rogers, B. M., et al. (2017). Global fire emissions estimates during 1997–2016. *Earth System Science Data*, *9*, 697–720. https://doi.org/10.5194/essd-9-697-2017

Vlemmix, T., Hendrick, F., Pinardi, G., Smedt, I. D., Fayt, C., Hermans, C., et al. (2015). MAX-DOAS observations of aerosols, formaldehyde and nitrogen dioxide in the Beijing area: comparison of two profile retrieval approaches. *Atmospheric Measurement Techniques*, *8*(2), 941–963. https://doi.org/10.5194/amt-8-941-2015

Wang, Y., Beirle, S., Lampel, J., Koukouli, M., De Smedt, I., Theys, N., et al. (2017). Validation of OMI, GOME-2A and GOME-2B tropospheric NO2, SO2 and HCHO products using MAX-DOAS observations from 2011 to 2014 in Wuxi, China: Investigation of the effects of priori profiles and aerosols on the satellite products. *Atmospheric Chemistry and Physics*, *17*, 5007–5033. https://doi.org/10.5194/acp-17-5007-2017

Wert, B. P., Trainer, M., Fried, A., Ryerson, T. B., Henry, B., Potter, W., et al. (2003). Signatures of terminal alkene oxidation in airborne formaldehyde measurements during TexAQS 2000. *Journal of Geophysical Research*, *108*(D3), 4104. https://doi.org/10.1029/2002JD002502

Wiedinmyer, C., Akagi, S. K., Yokelson, R. J., Emmons, L. K., Al-Saadi, J. A., Orlando, J. J., & Soja, A. J. (2011). The Fire INventory from NCAR (FINN): A high resolution global model to estimate the emissions from open burning. *Geoscientific Model Development*, *4*, 625–641. https://doi.org/10.5194/gmd-4-625-2011

Wittrock, F., Richter, A., Oetjen, H., Burrows, J. P., Kanakidou, M., Myriokefalitakis, S., et al. (2006). Simultaneous global observations of glyoxal and formaldehyde from space. *Geophysical Research Letters*, *33*, L16804. https://doi.org/10.1029/2006GL026310

Xie, H., Du, L., Liu, S., Chen, L., Gao, S., Liu, S., et al. (2016). Dynamic monitoring of agricultural fires in China from 2010 to 2014 using MODIS and GlobeLand30 data. *ISPRS International Journal of Geo-Information*, *5*(10), 172. https://doi.org/10.3390/ijgi5100172

Zhang, L., Liu, Y., & Hao, L. (2016). Contributions of open crop straw burning emissions to PM2.5 concentrations in China. *Environmental Research Letters*, *11*. https://doi.org/10.1088/1748-9326/11/1/014014

Zheng, B., Tong, D., Li, M., Liu, F., Hong, C., Geng, G., et al. (2018). Trends in China's anthropogenic emissions since 2010 as the consequence of clean air actions. *Atmospheric Chemistry and Physics*, *18*, 14,095–14,111. https://doi.org/10.5194/acp-18-14095-2018

Zhu, L., Jacob, D. J., Keutsch, F. N., Mickley, L. J., Scheffe, R., Strum, M., et al. (2017). Formaldehyde (HCHO) as a hazardous air pollutant: Mapping surface air concentrations from satellite and inferring cancer risks in the United States. *Environmental Science & Technology*, *51*, 5650–5657. https://doi.org/10.1021/acs.est.7b01356

Zhu, L., Jacob, D. J., Kim, P. S., Fisher, J. A., Yu, K., Travis, K. R., et al. (2016). Observing atmospheric formaldehyde (HCHO) from space: Validation and intercomparison of six retrievals from four satellites (OMI, GOME2A, GOME2B, OMPS) with SEAC^{4}RS aircraft observations over the southeast US. *Atmospheric Chemistry and Physics*, *16*(21), 13,477–13,490. https://doi.org/10.5194/acp-16-13477-2016

Zhu, L., Jacob, D. J., Mickley, L. J., Marais, E. A., Cohan, D. S., Yoshida, Y., et al. (2014). Anthropogenic emissions of highly reactive volatile organic compounds in eastern Texas inferred from oversampling of satellite (OMI) measurements of HCHO columns. *Environmental Research Letters*, *9*, 114004. https://doi.org/10.1088/1748-9326/9/11/114004

Zhu, L., Mickley, L. J., Jacob, D. J., Marais, E. A., Sheng, J., Hu, L., et al. (2017). Long-term (2005–2014) trends in formaldehyde (HCHO) columns across North America as seen by the OMI satellite instrument: Evidence of changing emissions of volatile organic compounds. *Geophysical Research Letters*, *44*, 7079–7086. https://doi.org/10.1002/2017GL073859

Zhuang, Y., Li, R., Yang, H., Chen, D., Chen, Z., Gao, B., & He, B. (2018). Understanding temporal and spatial distribution of crop residue burning in China from 2003 to 2017 using MODIS data. *Remote Sensing*, *10*, 390. https://doi.org/10.3390/rs10030390